



Solution processed single-emissive-layer white organic light-emitting diodes based on fluorene host: Balanced consideration for color quality and electroluminescent efficiency



Shang-hui Ye^{a,*}, Tian-qing Hu^a, Zhou Zhou^a, Min Yang^a, Qun-bo Mei^a, Yun-qi Liu^{b,**}, Li-ping Liu^a, Bang-cheng Zhai^a, Zhen-hong Jia^a, Wei Huang^{a,c}

^a Key Laboratory for Organic Electronics and Information Displays & Institute of Advanced Materials (IAM), Jiangsu National Synergetic Innovation Center for Advanced Materials (SICAM), Nanjing University of Posts & Telecommunications, 9 Wenyuan Road, Nanjing 210023, China

^b Beijing National Laboratory for Molecular Sciences (BNLMS), Institute of Chemistry, Chinese Academy of Sciences, Beijing 100190, China

^c Key Laboratory of Flexible Electronics (KLOFE) & Institute of Advanced Materials (IAM), Jiangsu National Synergetic Innovation Center for Advanced Materials (SICAM), Nanjing Tech University (NanjingTech), 30 South Puzhu Road, Nanjing 211816, China

ARTICLE INFO

Article history:

Received 27 November 2014

Received in revised form

16 March 2016

Accepted 19 March 2016

Available online 31 March 2016

Keywords:

Solution processing

White OLEDs

Color-rendering index

Solid-state lighting

Single-emissive-layer

ABSTRACT

Cost-effective fabrication of white organic light-emitting diodes (WOLED) is meaningful toward commercial application of environment-friendly solid-state lighting sources. Electroluminescent efficiency and color quality are two opposite performance characteristics facing solution processed WOLEDs requiring balanced consideration. Herein, a recently synthesized molecule of 4,4'-(9,9'-(1,3-phenylene)bis(9H-fluorene-9,9-diyl))bis(N,N-diphenylaniline) (DTPAFB) is introduced as a host material for solution processed all-phosphor WOLEDs, embracing four well-known molecules which are blue iridium (III) bis(2-(4,6-difluorophenyl)pyridinato-N,C²)(picolate) (Flrpic), green iridium (III) bis[2-(2-pyridinyl-N-phenyl-C)(2,4-pentanedionato-O²,O⁴)] [Ir(ppy)₂(acac)], and orange iridium (III) bis(2-phenyl-benzothiazole-C²,N)(acetylacetonate) [Ir(bt)₂(acac)] plus a home-made red phosphor of iridium (III) tris(1-(2,6-dimethylphenoxy)-4-(4-chlorophenyl)phthalazine) [Ir(MPCPPZ)₃]. Illumination quality white light with high brightness, high efficiency, suitable correlated color temperature (CCT), high color-rendering index (CRI), and stable electroluminescent (EL) emission is obtained. A stable white emission with a CRI over 70, Commission Internationale de L'Eclairage (CIE) of (0.37, 0.42), and high EL efficiency of 19.6 lm W⁻¹ at high luminance of 2000 cd m⁻² for blue/orange complementary color WOLEDs is demonstrated. The optimized red/green/blue three primary color WOLEDs show improved CRI up to 81, moderate high efficiency of 25.8 cd A⁻¹, 14.4 lm W⁻¹, and EQE of 13.9%. Furthermore, the red/green/blue/orange four primary color WOLEDs show the optional balance between color quality and EL efficiency with high CRI of around 81–83 and medium CCT of 3755–3929 K which is warm and soft to human eyes. At an illumination relevant luminance of 1000 cd m⁻², the total power efficiency reaches 33.6 lm W⁻¹, and still remains 30.2 lm W⁻¹ at 3000 cd m⁻², approaching the efficiency of state-of-the-art fluorescent-tube (40–70 lm W⁻¹), potentially suitable as an environment-friendly solid-state lighting source. This work indicates that developing high performance host materials and highly efficient phosphors and carefully combining them with common phosphors is an effective way toward high performance WOLEDs.

© 2016 Elsevier B.V. All rights reserved.

1. Introduction

White organic light-emitting diodes (WOLEDs) featured by

high-quality color, energy-saving properties, ease of large-area fabrication, bio-friendly diffusive warm light, and freedom from radiation damage have witnessed the emerging and dramatic development for commercial lighting panel models. It has been generally recognized as the most promising candidate as a next generation lighting technique [1].

As for a solid-state lighting source, two primary parameters must be taken into account: one is the electroluminescent (EL)

* Corresponding author.

** Corresponding author.

E-mail addresses: iamshye@njupt.edu.cn (S.-h. Ye), liuyq@iccas.ac.cn (Y.-q. Liu).

efficiency, and the other is color quality.

To obtain high efficiency, phosphors are always introduced into the emissive layer due to the spin-coupling effect, which gives them the ability to harvest both singlet and triplet excitons leading to nearly 100% internal quantum efficiency [2–4]. To achieve white emission, more than one luminophore is utilized. The dominating approach is to combine the electroluminescence from blue, green, and red luminophores which leaves some freedom in how the luminophores are combined, i.e., whether they are blended in a single layer, separated into different layers of the same OLEDs, or contained in several formally independent devices each of which emits different colors [5]. In principle, tandem WOLEDs by red, green, and blue (RGB) emitters can improve the operation stability, but the spectral instability due to high energy exciton of the blue emitter makes it problematic [6–8]. In contrast, single-emissive-layer from RGB blend is more advantageous for stable white electroluminescence emissions change as the operating voltage increases, free from problematic recombination zone-shifting [9]. This leads to brightness-dependent color-shifts [10]. In regards to the components of the emissive layer, blue and orange (BO) or yellow (BY) two complementary color WOLEDs are generally more efficient than the RGB three primary color types. In this system the phosphors are commonly dispersed into a host material to avoid concentration annihilation and triplet-triplet quenching, and thus a suitable combination of highly efficient phosphors with a proper host material is equally important [11].

Apart from electroluminescent (EL) efficiency, color quality is another important factor to be considered, which involves EL spectrum, color-rendering index (CRI), Commission Internationale de L'Eclairage chromaticity coordinates ($CIE_{x,y}$), and correlated color temperature (CCT). The EL spectrum should cover the entire visible region (400–700 nm), CRI around 70 for general lighting source, $CIE_{x,y}$ in the white color region, and CCT between 2500 K and 6000 K [12]. In general, WOLEDs based on BO complementary emitters always exhibit moderate color quality with intermediate CRI in the range of 52–65, compared with RGB three primary color devices. Obviously, the more primary components the emitting layer contains, the better the EL color quality will become. Therefore, red, green, blue, and orange (GRBO) four primary color WOLEDs possess even better color quality to their RGB counterpart.

As a result, a balanced consideration should be addressed between color quality and EL efficiency. For common phosphors and host materials, optimizing one physical parameter often frustrates other aspects, leaving a limited space for optimization. However, combining newly developed materials with common small host materials [13,14] brings a bright hope to this field.

In 2008, Cao's group utilizing poly(9-vinyl carbazole) (PVK) host coupled with blue and red phosphors fabricated a RB WOLED with a CRI of 52 and EL efficiency of 16.1 cd A^{-1} , and an RGB WOLED with a CRI of 77 and an EL efficiency of 24.3 cd A^{-1} [15]. In 2009, this group recorded an efficiency of 42.9 cd A^{-1} by doping the PVK host with a home-made yellow phosphor and the commonly used sky-blue Iridium complex, Flrpic, iridium (III) bis(2-(4,6-difluorophenyl)pyridinato- N,C^2)(picolinate). Yet the resulting moderate color quality with CRI falling in the narrow range of 52–55 is not impressive [16]. In 2012, Wang et al. reported extremely high-performance solution-processed BO WOLEDs, establishing a new world record efficiency of 70.6 cd A^{-1} , 47.6 lm W^{-1} , and 26.0% at 100 cd m^{-2} with a CRI of 62 by incorporating a new dendritic carbazole host material with a home-made orange-emitting iridium complex plus a low-conductivity PEDOT:PSS [17]. Yet the color quality still needs enhancement. In 2013, Xie's group employed a bipolar transport host of diphenylphosphoryl fluorene derivative doped with the common RGB emitters and fabricated warm WOLEDs with a power efficiency of 12.95 lm W^{-1} and a CRI of

82 at high luminance of 1594 cd m^{-2} [18].

WOLEDs possessing both good color quality and high efficiency, especially at high brightness is a demanding challenge facing the solution processing method.

Recently, Xu and his coworkers reported single-emissive-layer BO WOLEDs and obtained high efficiency of 28.3 cd A^{-1} at high luminance of 5000 cd m^{-2} by employing a newly synthesized orange phosphor [19]. In 2013, Xie and colleagues synthesized a new deep red phosphorescent dye Ir(pmiq)₂(acac) and fabricated high quality WOLEDs with ultra-high CRI up to 95, power efficiency of 7.86 lm W^{-1} and high luminance of 2529 cd m^{-2} at 5 V [20]. Recently, this team synthesized a new green-yellow (GY) phosphorescent Iridium complex and fabricated three-component WOLEDs with very high CRI above 85 and improved power efficiency of 10.4 lm W^{-1} [21]. Yang's group proposed tetraarylsilane host materials and fabricated highly efficient WOLEDs with a peak power efficiency of 47.2 lm W^{-1} and a CRI of 58–60 [22]. Inverted device architecture from common emitters toward stable WOLEDs was developed by Colsmann and his coworkers with stable EL efficiency of 18 cd A^{-1} and a CRI of 75 at a large luminance regime between 1500 and 7500 cd m^{-2} [23]. This tremendous progress makes us believe that the cost-effective WOLEDs will become accessible for general applications in the near future.

In this article, we introduce a home-made host material of 4,4'-(9,9'-(1,3-phenylene)bis(9H-fluorene-9,9-diyl)) bis(*N,N*-diphenylamine) (DTPAFB) and fabricated single-emissive-layer WOLEDs through the simple solution processing method by embracing four common molecules which are blue Flrpic, green iridium (III) bis[2-(2-pyridinyl-*N*)phenyl-C](2,4-pentanedionato- O^2, O^4) [Ir(ppy)₂(acac)], and orange iridium (III) bis(2-phenyl-benzothiazole- C^2, N)(acetylacetonate) [Ir(bt)₂(acac)], plus a home-made red phosphor of iridium (III) tris(1-(2,6-dimethylphenoxy)-4-(4-chlorophenyl)phthalazine) [Ir(MPCPPZ)₃]. DTPAFB host possesses more suitable energy level alignment (for details, see Fig. 1) compared to a PVK host material. The binary BO complementary color WOLEDs show stable EL emission with a high CRI over 70 and relatively high luminance efficiency of 26.3 cd A^{-1} and power efficiency of 19.6 lm W^{-1} . The optimized RGB three-component WOLEDs show improved CRI up to 81 with the maximum luminous efficiency of 25.8 cd A^{-1} , 14.4 lm W^{-1} , and external quantum efficiency (EQE) of 13.9%. Furthermore, we have studied RGBO four primary color WOLEDs and obtained good results with high EL efficiency of 28.9 cd A^{-1} , 17.4 lm W^{-1} , and EQE of 13.1% which is comparable to some thermally deposited multiply doped WOLEDs. At the illumination-relevant luminance of 1000 cd m^{-2} , the total power efficiency reaches 33.6 lm W^{-1} , and still remains 30.2 lm W^{-1} at 3000 cd m^{-2} , approaching the efficiency of state-of-the-art fluorescent-tube ($40\text{--}70 \text{ lm W}^{-1}$), potentially suitable for environment-friendly solid-state lighting sources.

2. Experimental

2.1. Materials

TPBI and PVK were purchased from Aldrich, while OXD-7, Flrpic, Ir(ppy)₂(acac), and Ir(bt)₂(acac) were purchased from Luminescence Technology Corp, and the red phosphors of Ir(MPCPPZ)₃ and DTPAFB were synthesized by our group. Polyethylenedioxythiophene:polystyrene sulfonate (Baytron Clevis A14083, Bayer AG), PEDOT:PSS, was commercially available and used as received.

2.2. Characteristics

UV–vis absorption and fluorescence spectra were collected with Hitachi U3010 and Hitachi F-4500 spectrophotometers,

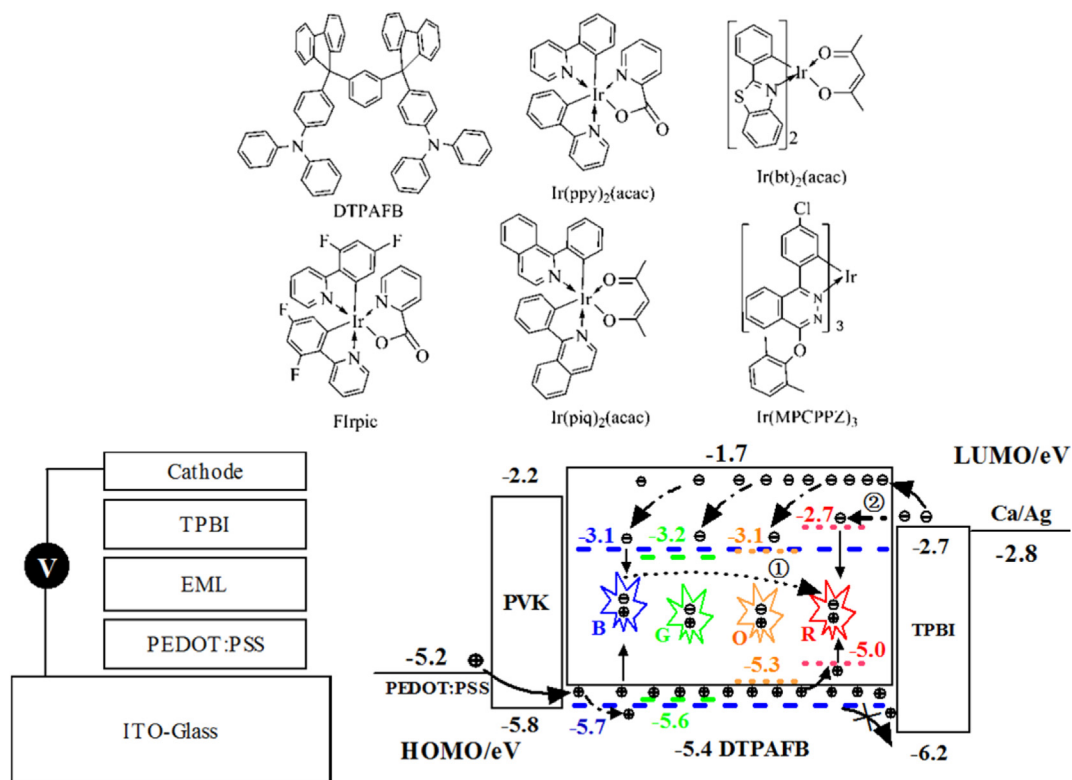


Fig. 1. Device structure, energy level diagram, and molecular structures of the related materials used in this study: DTPAFB, Flrpic, Ir(ppy)₂(acac), Ir(bt)₂(acac), Ir(piq)₂(acac), and Ir(MPCPPZ)₃.

respectively. Transient photoluminescence decay measurements were carried out by using time-correlated single-photon counting lifetime spectroscopy system Edinburgh FL920 coupled with a semiconductor laser, hydrogen lamp, or Xe lamp as the excitation source ($\lambda_{\text{ex}} = 308$ nm). A quartz crystal oscillator placed near the substrate was used to monitor the thickness of thermally deposited layers, which was calibrated *ex situ* using an Ambios Technology XP-2 surface profilometer. Tapping mode atomic force microscope (AFM) imaging was carried out on four randomly chosen spots.

2.3. Device fabrication and measurements

In the general procedure, indium tin oxide (ITO)-coated glass substrates were etched, patterned, and washed with detergent, deionized water, acetone, and ethanol in turn. PEDOT:PSS was spin-coated to smooth the ITO surface and to promote hole injection, and then the emissive layer was spin-coated from a chlorobenzene solution on which an electron-transporting/hole-blocking layer was deposited in a vacuum chamber at a pressure of 8×10^{-5} Pa. In all devices, a thin (8 Å) calcium layer served as the electron-injecting layer at the Ag electrode interface, and a 100 nm thick Ag capping layer was deposited through a shadow mask. The active area of the device was 6 mm². EL spectra were collected by the Hitachi F-4500 spectrophotometer, and chromaticity coordinates were measured with a SpectraScan PR655 photometer. Current density-voltage-luminance (*J-V-L*) measurements were recorded simultaneously using a Keithley 4200 semiconductor parameter analyzer coupled with a Newport multifunction 2835-C optical meter, measuring luminance in the forward direction. All device characterizations were carried out under ambient laboratory air at room temperature.

The hole-only device is fabricated in the configuration of ITO/

PEDOT:PSS/DTPAFB:OXD-7:Ir(piq)₂(acac) (65 nm)/Au, and electron-only device's structure is ITO/Al/DTPAFB:OXD-7:Ir(piq)₂(acac) (65 nm)/TPBI (30 nm)/Ca/Ag.

3. Results and discussion

3.1. Photophysical properties

For the home-made host material of DTPAFB, its synthesis, single crystal structure, and electrochemical properties have been demonstrated in a recently published paper, along with the primary application in a highly efficient sky-blue phosphorescent OLED [24].

The ultraviolet–visible (UV–Vis) absorption spectra of RGBO phosphors are shown in Fig. 2, along with the photoluminescent (PL) spectra of the DTPAFB host. It can be seen that these phosphors have strong absorption peaks in the short wavelength region around 300 nm, which is ascribed to the ligand–ligand π – π transition and a relatively strong absorption band from 350 to 450 nm arising from the singlet metal-to-ligand charge transfer (¹MLCT), plus an intermediate or weak absorption extending over 450 nm, which can be assigned to the spin-forbidden triplet metal-to-ligand charge transfer (³MLCT). These transitions are well overlapped with the emission spectrum of DTPAFB, and thus efficient Förster energy transfer can be anticipated [25].

Also, the EL spectra of the monochromatic devices of the related phosphors are presented in Fig. 2b. The blue phosphor of Flrpic shows an emission peak at 471 nm, along with a strong shoulder at 500 nm. The Ir(ppy)₂(acac) phosphor displays green emission with a peak at 521 nm and a shoulder at 547 nm. The Ir(bt)₂(acac) emitter exhibits strong orange emission peaked at 560 nm, accompanied by a shoulder at around 596 nm. The typical red

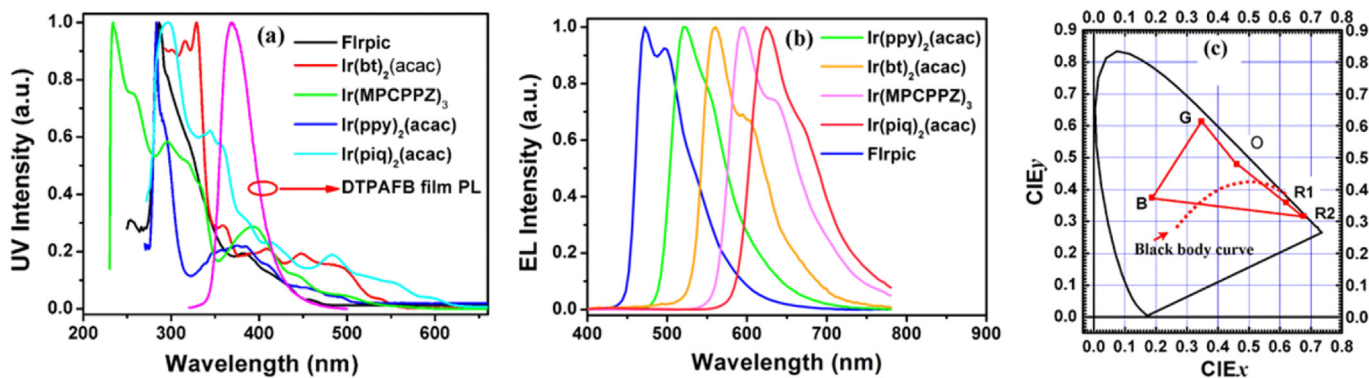


Fig. 2. Photophysical properties of the blue, green, orange, and red phosphors, along with DTPAFB host material in dilute dichloromethane solution (1×10^{-6} mol L⁻¹): (a) UV–Vis absorption spectra of the phosphors and the photoluminescence spectra of DTPAFB host material; (b) EL spectrum of the monochromatic device; (c) the CIE_{xy} coordinate diagrams. (For interpretation of the references to color in this figure legend, the reader is referred to the web version of this article.)

phosphor of Ir(pi q)₂(acac) features saturated red emission possessing a main peak at 624 nm and a shoulder at around 670 nm. As for the home-made Ir(MPCPPZ)₃ phosphor, it shows red emission with the main peak at 596 nm and a strong shoulder at 633 nm. It should be noted that Ir(MPCPPZ)₃ is a highly efficient red phosphor exhibiting almost 100% internal quantum yield in the red OLEDs [26], while the conventional Ir(pi q)₂(acac) red emitter only shows an EQE of 6.9% [15]. These RGBO phosphors, covering the whole visible spectrum region, provide multiple choices for WOLEDs construction, and the large overlapping with the black body curve makes high quality complex white lighting possible (Fig. 2c).

3.2. Host-guest-system

To explore the triplet exciton confinement properties of DTPAFB as a host material and understand the energy transfer mechanism, transient decay spectra were studied on a series of the doped films. The doping content is 10 wt% for Flrpic phosphor, and 2 wt% for Ir(ppy)₂(acac), Ir(bt)₂(acac), Ir(pi q)₂(acac) and Ir(MPCPPZ)₃ complexes, respectively. All the samples were excited at the absorption peak of DTPAFB (308 nm) and were detected at the corresponding emission peaks. Fig. 3 depicts the experimental results along with the simulated curves. All the transient decay plots were fitted exponentially by

$$I_{PL}(t) = A_1 e^{-\tau_1/t} + A_2 e^{-\tau_2/t} \quad (1)$$

where I_{PL} is the photoluminescent intensity, A_1 and A_2 are quantities of the emission components, t is decay time, and τ_1 and τ_2 are the lifetimes of the corresponding emission components [27]. For

the Flrpic blend film, it exhibits a biexponential decay, in which the first lifetime is 74.3 ns, while the second lifetime is 484.0 ns, and the emission components are 79.1% and 20.9% for τ_1 and τ_2 , respectively (for details, see Table 1). Compared with other host-guest systems (around 1.4 μ s) [28,29], Flrpic guest shows relatively shorter lifetime, which may be affected by the DTPAFB host with a short lifetime of 2.35 ns (for details, refer to Fig. S1). Two components indicate a weak energy back-transfer from the guest site to the matrix site. For the monochromatic blue phosphorescent device, this reverse process may cause efficiency loss. However, for WOLEDs, the energy back-transferred onto the matrix can still be harvested by other emitters with lower triplet energy levels, and thus not reduce the internal quantum efficiency. This mechanism is like the hybrid concept of WOLEDs, which combines blue fluorescent with green and red phosphorescent emitters, rendering unity internal quantum efficiency [30,31]. A similar phenomenon has also been demonstrated in the literature by Leo's group [32]. As far as the green Ir(ppy)₂(acac) phosphor is concerned, it shows a monoexponential decay behavior with a lifetime of 1045.2 ns, suggesting complete energy transfer from the host to the guest. A similar behavior is also observed for the orange Ir(bt)₂(acac) and red Ir(pi q)₂(acac) phosphors, featuring a comparable lifetime of 932.0 and 970.1 ns, respectively. However, the home-made Ir(MPCPPZ)₃ red phosphor displays a very long lifetime of 1677.8 ns, obviously longer when compared to the neat-thin film state (around 1 μ s) [26], which accounts for its high photoluminescent quantum efficiency ($\Phi_{PL} = 95.3\%$). From the above analysis we can anticipate the DTPAFB molecule to be an efficient host material for WOLEDs.

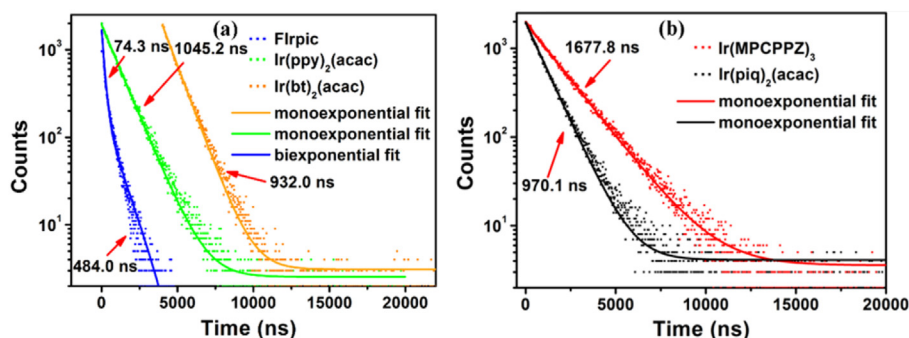


Fig. 3. Transient photoluminescent decay curves of DTPAFB solid thin films excited at 308 nm at room temperature: (a) doped with 10 wt% Flrpic, 2 wt% Ir(ppy)₂(acac), and Ir(bt)₂(acac); (b) 2 wt% Ir(MPCPPZ)₃ and Ir(pi q)₂(acac). The transient curves are shifted along the axis for better visibility.

Table 1Fitted exponential decay curves of the transient photoluminescent spectra of Flrpic, Ir(ppy)₂(acac), Ir(bt)₂(acac), Ir(piq)₂(acac), and Ir(MPCPPZ)₃ doped in DTPAFB host material.

Materials	τ_1 (ns)	A_1	$A_1/(A_1+A_2)$ (%)	τ_2 (ns)	A_2	$A_2/(A_1+A_2)$ (%)
Flrpic	74.3	2178.5	79.1	484.0	575.3	20.9
Ir(ppy) ₂ (acac)	1045.2	1928.6	100	0	0	0
Ir(bt) ₂ (acac)	932.0	140094.4	100	0	0	0
Ir(piq) ₂ (acac)	970.1	1953.5	100	0	0	0
Ir(MPCPPZ) ₃	1677.8	1958.1	100	0	0	0

3.3. Thin film morphologies

Apart from the spectrum-matching and suitable energy level alignment, high quality film of the thin-film based device is also important for efficient charge injection and transportation and stable EL emission, and thus we turn our attention to the surface morphology. In general, the more stable the thin film, the higher the performance of the WOLED. Therefore, we explored the DTPAFB thin films of the same active layer of the RGBO WOLEDs by atomic force microscopy (AFM) images. The sample was baked at 120 °C for 1 h under nitrogen atmosphere. For comparison, we also prepared unbaked films with results shown in Fig. 4. The DTPAFB sample shows very smooth and amorphous surfaces, with a room-mean-square (RMS) roughness of 0.757 nm in the pristine thin-film state. After annealed for 1 h it displays an even smoother surface than that of the pristine state, with a RMS value of 0.446 nm. To clearly profile the surface morphology, we can refer to the cross section of the randomly chosen trace, marked as the red line in Fig. 4b. The corresponding trace of the pristine film is showed in Fig. 4c with a R_{\max} of 3.450 nm and a R_z of 2.598 nm. Meaningfully, the baked film shows lower roughness with a reduced R_{\max} and R_z of 2.016 nm and 1.433 nm, respectively, as shown in Fig. 4c and 4f. Thermally promoted surface morphology upon annealing is a typical characteristic of the amorphous material. In the phase images, no aggregation, microcrystallization, or phase separation

occurs in both samples, which means all the doped phosphors are homogeneously dispersed in the DTPAFB host material. This result indicates that DTPAFB possesses excellent film-forming ability and miscibility to the RGBO phosphors as well as morphological stability which is advantageous for device fabrication.

3.4. Two-color white OLEDs

Excellent compatibility and film-forming ability, suitable energy level alignment, and matched spectra between DTPAFB and the RGBO phosphors encouraged us to explore device applications. Firstly, we chose the sky-blue phosphor, Flrpic, and the orange phosphor, Ir(bt)₂(acac), as the two primary dyes for good spectrum-matching and high efficiency. For comparison, we also prepared the PVK device in the same device architecture of ITO/PEDOT:PSS (35 nm)/EML (65 nm)/TPBI (35 nm)/Cathode, in which EML comprises Flrpic and Ir(bt)₂(acac) doped in DTPAFB or PVK host material (for details, see Fig. 1). Trace of OXD-7 (30 wt%) was added in the EML to balance the hole/electron charge-carrier flux. Firstly, we optimized the Flrpic doping content as 10% weight ratio for the monochromatic blue emission, and then systematically tuned the Ir(bt)₂(acac) doping level to adjust the white emission spectrum.

The optimized orange content is 0.36 wt% for warm white emission with EL spectra shown in Fig. 5. It can be seen that the DPAFB device shows stable emission under the applied voltages

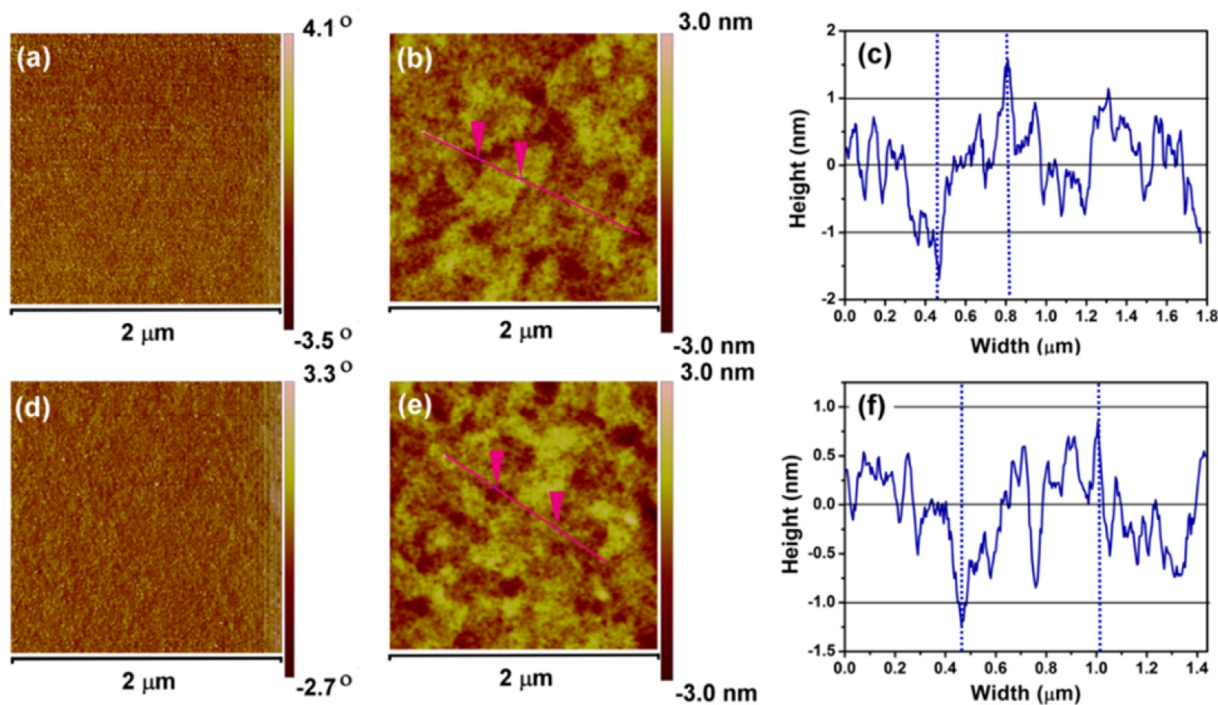


Fig. 4. AFM images of DTPAFB films doped with RGBO four phosphors on ITO-glass substrate: (a) phase images, (b) height images, (c) section profile along the red line as marked in figure b of the spin-coated films (up layer), and baked under nitrogen atmosphere at 120 °C for 1 h (d, e, f, lower layer). (For interpretation of the references to color in this figure legend, the reader is referred to the web version of this article.)

ranging from 5 to 11 V, with CIE_{x,y} chromaticity coordinates shifting a little of $\pm(0.003, 0.005)$ at 5 V of (0.375, 0.440) to (0.372, 0.435) at 11 V, CCT around 4500, and the corresponding brightness increases from around 500 to 30,000 cd m⁻². Highly stable EL emission against voltage increase indicates that (1) the recombination zone does not shift, (2) the EL mechanism does not change in the emissive layer. To carefully check the EL spectrum, we find the blue component increases a little with increasing operating voltage, suggesting that the trapping site is saturated under high current injection and charge trapping by the lower energy site of orange phosphor is not significant [5,33]. Another thing worth mentioning is the wide spectra-covering region from around 450 to 700 nm, and thus high CRI value of 68–71. For a typical fluorescent lamp, it has a CRI rating between 60 and 99 [34]. To the best of our knowledge, such high color rendering index WOLED is seldom reported from blue/orange complementary phosphors, whose CRI always fall in a low range of 50–60 [16,17,35–37]. We attribute the stable EL and high CRI of our white device to the well matched spectra of the blue and orange iridium complexes, and to the carefully optimized doping ratio, plus good surface morphology stability of DTPAFB host material.

The current density-voltage-luminance (*J-V-L*) curves are depicted in Fig. 5. In general, the DTPAFB device shows lower driving voltage than the PVK device, with a turn-on voltage (V_{on} , recorded at 1 cd m⁻²) of 3.1 V, compared with 4.5 V of the PVK device, which can be attributed to the better matched energy level alignment of the DTPAFB device than that of the PVK device (for details, see Fig. 1); they all show comparable high maximum brightness of around 30,000 cd m⁻². Meaningfully, DTPAFB device exhibits higher efficiency with the maximum current efficiency of 26.3 cd A⁻¹ and power efficiency of 19.6 lm W⁻¹, compared with 24.1 cd A⁻¹ and 10.9 lm W⁻¹ of PVK device. The maximum EQE is 10.5% and 9.6% for TPAFB and PVK devices, respectively. Moreover, the maximum efficiency occurs in the brightness range of 100–3000 cd m⁻², which is more meaningful for practical applications [38]. This result also indicates that carefully combining a suitable host material with high efficiency phosphors can

circumvent, to some extent, the efficiency roll-off problem at high brightness. At the illumination-relevant luminance of 1000 cd m⁻², it still retains a high efficiency of 26.1 cd A⁻¹ and 15.0 lm W⁻¹, making it even more comparable to some thermally deposited multilayer WOLEDs [40–43] among the most efficient WOLEDs based on solution processing technique [36,39]. For example, Cao's team also reported similar stable WOLEDs in a doubly-doped system for PVK-OXD-7 host with the maximum EQE of 10.0%, 16.1 cd A⁻¹, and 6.3 lm W⁻¹, but its CRI is only 52 [15]. Compared with the majority of other BO WOLEDs, our device shows a higher CRI value, hence better color quality. We can further enhance the EL efficiency by increasing the orange doping level, yet the color quality will decrease. Therefore, a balanced consideration was implemented for the two-component WOLEDs.

3.5. RGB three primary color WOLEDs

To improve the color quality of the white OLEDs, we turned our attention to blue-green-red (RGB) three primary color WOLEDs, which always exhibit a wide spectral covering region and high CRI value. The difficulty facing RGB device fabrication is how to definitely control the energy balance between the three components to achieve stable white emission. For the thermal deposition technique, it is very difficult to simultaneously control three or more components during vacuum deposition, but solution processing methods make it easy to perform. The device structure is the same as the BO WOLEDs, but only the EML is changed. Herein, Ir(*p-py*)₂(acac) and Ir(*piq*)₂(acac) are chosen for RG components. Using the optimized doping content of the monochromatic blue device, we only need to tune the RG doping levels. By adjusting the two components ratio, we fabricated a series of devices. Devices containing the typical red phosphor of Ir(*piq*)₂(acac) are named T1-T4 for short. Moreover, we exploited a home-made red phosphor of Ir(MPCPPZ)₃ to replace Ir(*piq*)₂(acac), for devices T5-T8, due to its well matched spectrum with the blue and green phosphors as well as due to its high efficiency.

Fig. 6 shows the EL spectra of RGB white devices T1-T4. Three

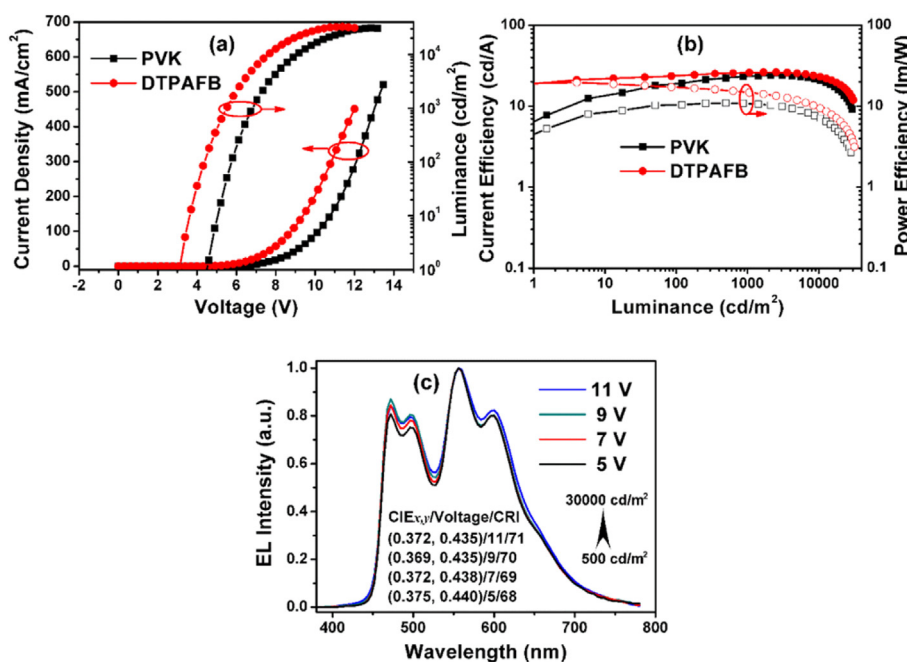


Fig. 5. *J-V-L* curves of the white OLEDs from the BO components (a), EL efficiency curves as a function of luminance (b), and EL spectra of DTPAFB device under variant driving voltages (c).

characteristic emission bands emerge at 471, 502, and 619 nm, which are featural emissions of the three RGB emitters. As the GR doping level increases, the EL spectrum becomes more full, and thus the CRI increases from 63 to 75, corresponding to a CCT of around 4819 to 4275, which is comparable to other studies. For example, Cao's group reported similar RGB WOLEDs with the CRI value of 77 and CCT of 5010 [15]. Also, the $CIE_{x,y}$ coordinates shift toward warm-light region from (0.354, 0.388) to (0.377, 0.421). It must be noted that in this RGB system, a big concave exists at around 578 nm, owing not only to the weak spectral overlap between GR emitters at the orange region, but also to the large overlap of the GB emitters at the green emission region at around 500 nm, which limits the doping level of the green dopant. Although we can increase the green emitter's doping level to enhance the spectrum-covering region to some extent, yet it simultaneously shifts the $CIE_{x,y}$ to the green region. So the doping level should be controlled below 0.15 wt%. For this RGB system based on FIrpic blue emitter, a high CRI value is limited to around 75, due to the lack of deep blue emission, which is unavailable from the commercial blue phosphorescent materials.

To improve the color quality, we introduced a home-made red phosphor, Ir(MPCPPZ)₃, in T5-T8 devices because of the good spectrum-matching with the BG emitters. As a result, the spectral quality shows significant improvement, and the concave at around 578 nm is well filled, as shown in Fig. 6b and 6d. For this series of devices, the EL spectrum shifts toward the warm-light region as the doping concentration increases. In the meanwhile, the CRI and $CIE_{x,y}$ coordinates have also been improved. For example, device T5 has a CRI of 78, and it has been enhanced to 79 for device T6, and to 81 for devices T7 and T8. The $CIE_{x,y}$ coordinates have also been shifted from (0.366, 0.417) for device T5 to (0.411, 0.416) for device T8 with the u-v Dev of only 0.0084 (for details, see Fig. 6), indicating negligible color difference from the Planckian locus. More importantly, the EL spectrum is stable against the increasing driving voltage. Let's use device T8 as an example: its $CIE_{x,y}$ are (0.424,

0.417) at 5 V, which shift a little of (0.013, 0.001) to (0.411, 0.416) at 9 V, corresponding to a brightness of around 400 to 20,000 $cd\ m^{-2}$. The u-v Dev also shows, at the same time, negligible change from 0.0074 to 0.0095 when the driving voltage increases from 5 to 9 V, and the corresponding CCT is around 3332–3581 K, very close to the morning sunlight featuring a CCT of around 3500 K. Such chromatic hue is suitable for a high quality lighting source.

The J-V-L characteristic curves of devices T5-T8 are plotted in Fig. 7, with key parameters listed in Table 2. In general, the turn-on voltage is closely related with the doping content. For Ir(piq)₂(acac) devices T1-T4, the V_{on} is around 3.3–3.5 V, with no obvious difference at high current density (for details, see Fig. S2). However, the current density decreases with increasing doping levels for devices T1-T3, but further increasing the doping content of Ir(p-py)(acac) to 0.2% in device T4 will lead to a current density rise. This suggests that the red dopant serves as a trapping center, which traps hole carriers from the host, and the trapped hole builds a space-charge field, which hinders charge transporting [33,44]. The trapped holes will recombine with the resonantly injected electrons on the red phosphor, form excitons, and radiate light, as shown in Fig. 1 marked as route 2. At the same time, triplet-triplet energy transfer from the high energy emitters, such as the blue and green phosphors, also functions, marked as route 1. The maximum brightness ranges from 26,742.3 to 31,967.1 $cd\ m^{-2}$ for devices T1-T4, which also increases with doping content, with the highest being device T3. Further increasing the doping level will result in brightness roll off, which may be attributed to triplet-triplet and/or concentration annihilation. The maximum luminous efficiency reaches 20.0 $cd\ A^{-1}$, 11.3 $lm\ W^{-1}$, and EQE of 11.3% for device T3; at 1000 $cd\ m^{-2}$ it still remains 19.5 $cd\ A^{-1}$, 10.8 $lm\ W^{-1}$, and EQE of 11.0%, more efficient compared with the previously reported RGB white OLEDs [15].

When a home-made red phosphor Ir(MPCPPZ)₃ was introduced in devices T5-T8, the EL performance was further improved. The V_{on} was reduced to around 3.0–3.2 V, and the maximum brightness

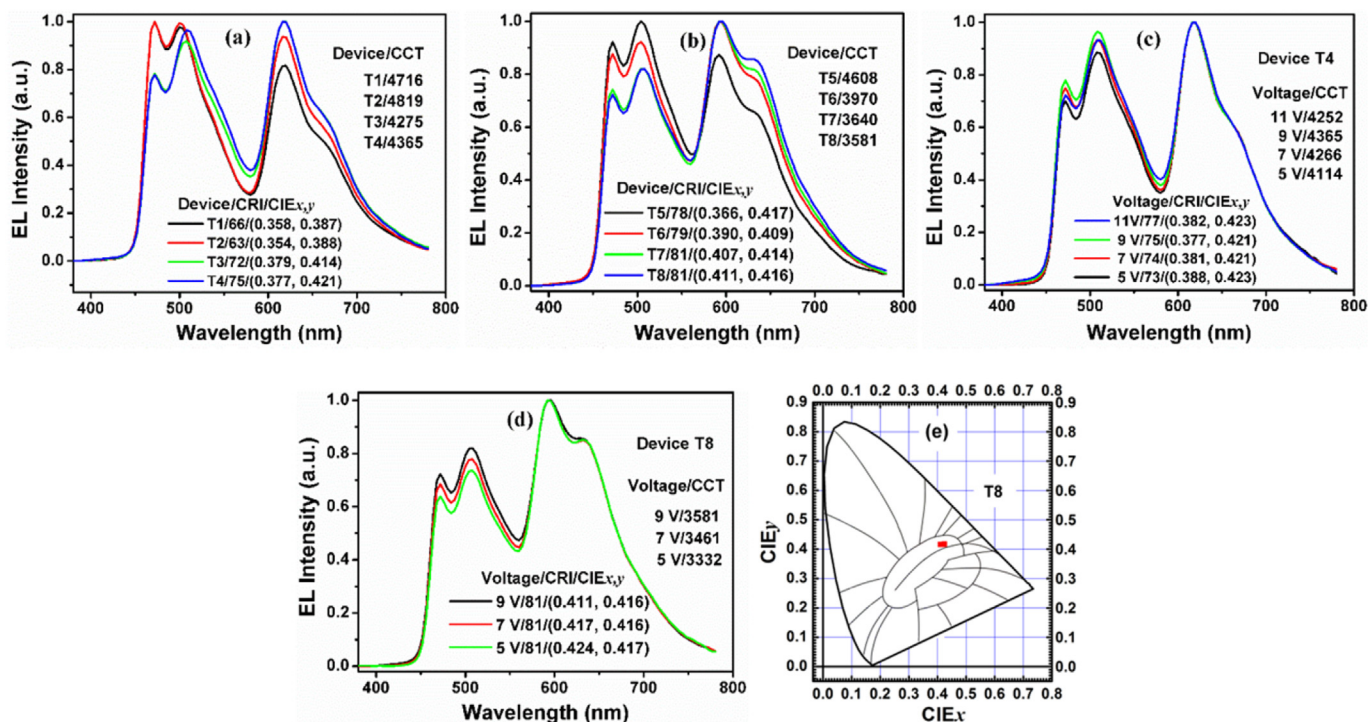


Fig. 6. The EL spectra of the RGB white OLEDs: (a) Ir(piq)₂(acac) based devices T1-T4 at 9 V; (b) Ir(MPCPPZ)₃ based Ir devices T5-T8 at 9 V; (c) EL characteristics of device T4 at variant driving voltages; (d) EL characteristics of device T8; (e) the corresponding $CIE_{x,y}$ chromaticity diagram of the white device T8.

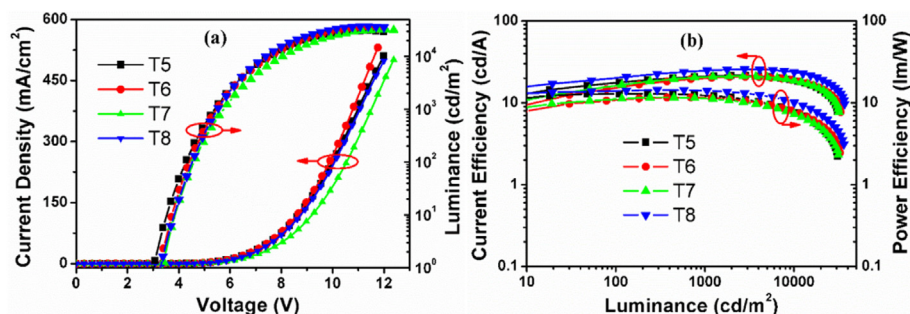


Fig. 7. EL characteristics of the RGB white OLEDs T5-8: (a) J - V - L curves; (b) EL efficiency as a function of luminance.

was improved to 33644.9 for T6 device, and 37048.6 cd m^{-2} for T8 device. The maximum luminous efficiency reached 25.8 cd A^{-1} , 14.4 lm W^{-1} , and EQE of 13.9% in device T8. Even at 1000 cd m^{-2} the EL efficiency still remained 24.8 cd A^{-1} , 14.1 lm W^{-1} , and EQE of 13.3%, comparable with thermally deposited multi-layer WOLEDs [45]. For example, in 2012, Leo's group reported a multilayer white OLED containing four phosphors with a CRI of 82, EQE of 10% at 1000 cd m^{-2} [32]. In comparison with $\text{Ir}(\text{piq})_2(\text{acac})$ devices, $\text{Ir}(\text{MPCPPZ})_3$ devices have around 30% enhancement in EL efficiency. On the whole, the efficiency roll-off at high luminance is low, which may arise from the balanced hole/electron carrier injection and transporting into the emissive layer and the broad exciton recombination zone in our single-emissive-layer device structure, compared to other double emissive layer white OLEDs [46,47]. More importantly, the EL color quality is also improved. We attribute the improvement to the high quantum efficiency of our home-made red phosphor, and to the well-matched emission spectrum between these RGB components. Therefore, based on the experimental results, the optimal doping ratio is (10:0.15:0.80) for this RGB WOLEDs, because the color quality and EL efficiency have reached their optimal values.

3.6. RGBO four primary phosphors white OLEDs

In principle, the color quality and EL efficiency of the RGB three primary color white system can be further improved by introducing the fourth primary emitter of orange phosphor, especially for $\text{Ir}(\text{piq})_2(\text{acac})$ WOLEDs due to the spectral concave at around 578 nm. So in this section we focused our attention on the RGBO four primary color WOLEDs by adding a highly efficient orange phosphor of $\text{Ir}(\text{bt})_2(\text{acac})$ in the EML. For thermal vacuum deposition method, it is very difficult to definitely co-evaporate four

phosphors and a host simultaneously. The solution processing method makes this step very easy to perform by just mixing them in solution and spin-coating to form the EML. The device structure is the same as the RGB white OLEDs, except that the EML comprises four phosphors. By definitely adjusting each component's content, two series of white devices were fabricated. One series of devices, containing $\text{Ir}(\text{piq})_2(\text{acac})$ red phosphor, are named Q1-Q4 for short, and the other containing $\text{Ir}(\text{MPCPPZ})_3$ red phosphor, are named Q5-Q8.

As expected, the color quality of $\text{Ir}(\text{piq})_2(\text{acac})$ devices demonstrated significant improvement. The spectral covering region has been further extended and, especially, the spectral concave in the orange region has been well filled, as shown in Fig. 8. So the CRI has been elevated to a satisfied value of around 74–83 in devices Q1-Q4, compared to RGB devices of around 73–77. The CRI value is closely related with the spectrum-covering region and reaches the highest of 83 in device Q4. The $\text{CIE}_{x,y}$ coordinates are around (0.364, 0.439) to (0.404, 0.410) for devices Q1-Q4, located in the warm-light region. And the CCT is around 3531–3732 K, very close to the natural sun light in the morning of 3500 K. It should be noted that the content of GO should be controlled below 0.03/0.22 wt%, or the CIE_y value will >0.42 , leading to big u-v Dev. For example, device Q4 with 0.03/0.22 wt% GO has a CIE_y of 0.410 and a negligible u-v Dev of around 0.0078 to 0.009 as the operation voltage increases from 5 to 10 V, covering a luminance range from 100 up to $20,000 \text{ cd m}^{-2}$; device Q2 with 0.03/0.25 wt% GO has a CIE_y of 0.431 and a big u-v Dev of around 0.0231–0.0212 under a bias of 5–10 V. For commercial application, the u-v Dev should be below 0.02.

For $\text{Ir}(\text{MPCPPZ})_3$ devices, the color quality has also been improved, but not significant when compared to $\text{Ir}(\text{piq})_2(\text{acac})$ series. For example, the CRI has improved from around 78–81 to 82 in devices Q6-7. The u-v Dev is around 0.015–0.014 for device Q7

Table 2
RGB white OLEDs performance parameters in device structure of ITO/PEDOT:PSS (35 nm)/[DTPAFB:OXD-7 (7:3)]: (10 wt%) Flrpic: $\text{Ir}(\text{ppy})_2(\text{acac})$: red phosphor (65 nm)/TPBI (35 nm)/Ca:Ag.

Device	Composition G/R	V_{on} [V]	LE [cd A^{-1}] ^a	PE [lm W^{-1}] ^a	L_{max} [cd m^{-2}] ^b	LE [cd A^{-1}] ^c	PE [lm W^{-1}] ^c	LE_{max} [cd A^{-1}] ^d	PE_{max} [lm W^{-1}]	EQE _{max} %
T1 ^e	0.08/0.26	3.3	17.9	9.8	27233.3 (464.3)	17.9	8.7	18.1 (2241.0)	10.6	10.5
T2 ^e	0.06/0.28	3.4	17.9	10.1	26742.3 (481.2)	18.0	8.9	18.2 (1595.9)	10.4	10.6
T3 ^e	0.15/0.30	3.4	19.5	10.8	31967.1 (446.0)	19.9	9.6	20.0 (1885.5)	11.3	11.3
T4 ^e	0.20/0.30	3.5	18.8	10.3	28403.6 (430.0)	18.9	9.1	19.1 (1941.8)	10.7	10.6
T5 ^f	0.15/0.50	3.0	21.1	12.3	30793.0 (434.4)	21.4	10.8	21.6 (1955.6)	13.0	10.5
T6 ^f	0.11/0.70	3.2	20.1	11.5	33644.9 (483.7)	20.8	10.5	20.9 (2839.6)	11.7	10.6
T7 ^f	0.15/0.70	3.2	20.7	11.3	31973.9 (460.0)	21.1	10.1	21.2 (2687.2)	11.7	10.9
T8 ^f	0.15/0.80	3.2	24.8	14.1	37048.6 (423.0)	25.7	13.0	25.8 (2785.4)	14.4	13.9

^a At 1000 cd m^{-2} .

^b The data in the bracket are the corresponding current density.

^c At 3000 cd m^{-2} .

^d The corresponding luminance.

^e $\text{Ir}(\text{piq})_2(\text{acac})$ red phosphor.

^f $\text{Ir}(\text{MPCPPZ})_3$ red phosphor.

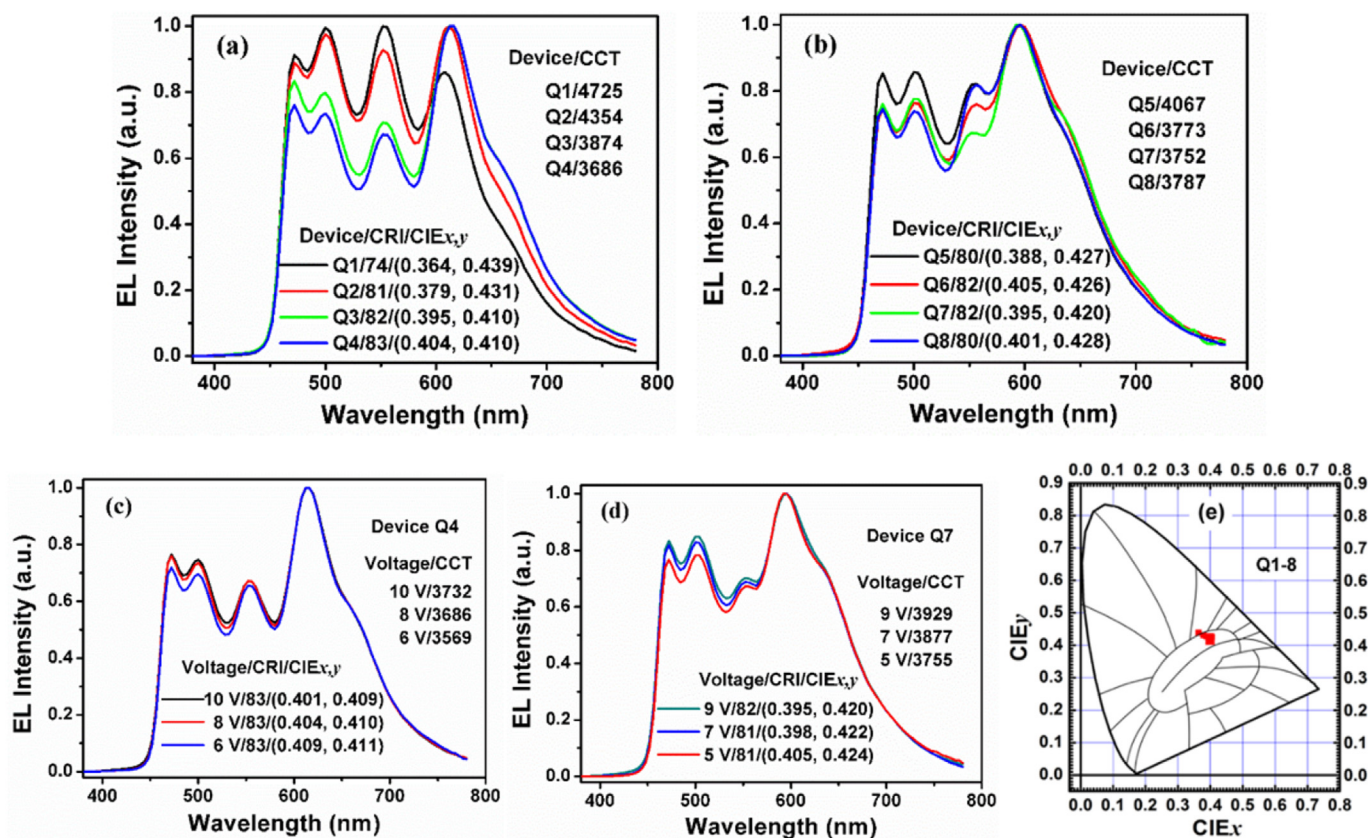


Fig. 8. The EL spectra of the RGBO white OLEDs: (a) Ir(piq)₂(acac) based devices of Q1–Q4 at 8 V; (b) Ir(MPCPPZ)₃ based devices of Q5–Q8 at 9 V; (c) EL characteristics of device Q4 at variant driving voltages; (d) EL characteristics of device Q7; (e) the corresponding CIE_{x,y} chromaticity diagram of both series of white devices of Q1–8.

biased with 5–9 V, the CIE_{x,y} are around (0.395, 0.420)–(0.405, 0.424), and the CCT is about 3755–3929 K, all located in the warm-white light region. Compared with multilayer thermally deposited RGBO WOLEDs, our devices show a more stable EL spectrum. On the whole, our white devices, whether two components, or three components and four components, show stable white emission in a large luminance range, whose work mechanism will be discussed in the following section.

Apart from the improved color quality, the EL performance has also been enhanced, which can be seen from the *J*-*V*-*L* curves in Fig. 9 and from Table 3. In general, the more content green and orange emitters have, the higher the performance of the device, because of the higher efficiency of GO phosphors. For example, device Q1 shows a current efficiency of 25.4 cd A⁻¹, power efficiency of 14.0 lm W⁻¹, and maximum brightness of

39,710.6 cd m⁻². Compared with the highest efficiency of RGB series of devices T1–T4, RGBO device of Q1 has around 25% improvement in EL efficiency, which can be attributed to the introduction of a highly efficient orange phosphor Ir(bt)₂(acac). The V_{on} is a little higher, around 3.5–3.9 V, compared with 3.3–3.5 V of T1–T4 series of devices. For Ir(MPCPPZ)₃ series of devices Q5–Q8, the performance improvement is more significant. The maximum current efficiency was improved to 28.9 cd A⁻¹, EQE of 13.1%, and power efficiency of 17.4 lm W⁻¹ for device Q5, comparable with some thermally deposited multiply doped WOLEDs. For example, Wong and his coworkers reported a multiply emissive layer WOLED with the maximum power efficiency of 18.5 lm W⁻¹ and EQE of 13.2% [48]. Xie's team demonstrated a series of multilayer WOLEDs with efficiency in the range of 21.9–31.4 cd A⁻¹ [49]. It is worth mentioning that the efficiency roll-off for our WOLEDs is very

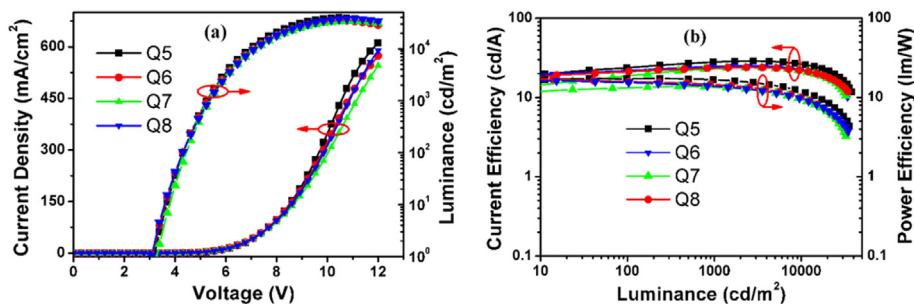


Fig. 9. (a) *J*-*V*-*L* curves of the RGBO white OLEDs based on Ir(MPCPPZ)₃ red phosphor; (b) efficiency curves as a function of luminance. (For interpretation of the references to color in this figure legend, the reader is referred to the web version of this article.)

Table 3
 RGBO white OLEDs characteristic parameters in the structure of ITO/PEDOT:PSS (35 nm)/[DTPAFB:OXD-7 (7:3)]:(10 wt%) Flrpic: Ir(ppy)₂(acac): red phosphor: Ir(bt)₂(acac) (65 nm)/TPBI (35 nm)/Ca:Ag.

Device	Doping content G/R/O	V _{on} [V]	LE [cd A ⁻¹] ^a	PE ^a [lm W ⁻¹]	L _{max} [cd m ⁻²] ^b	LE [cd A ⁻¹] ^c	PE ^c [lm W ⁻¹]	LE _{max} ^d [cd A ⁻¹]	PE _{max} [lm W ⁻¹]	EQE _{max} %
Q1 ^e	0.03/0.13/0.25	3.6	25.0	13.6	39710.6 (535.9)	25.3	12.5	25.4 (2502.5)	14.0	10.9
Q2 ^e	0.03/0.22/0.25	3.5	19.6	10.9	33221.6 (465.0)	20.1	9.9	20.8 (3949.4)	11.0	9.6
Q3 ^e	0.03/0.22/0.22	3.5	19.8	11.2	27806.5 (453.2)	19.7	9.7	20.0 (1787.4)	11.6	10.4
Q4 ^e	0.03/0.24/0.22	3.9	18.9	9.6	29626.0 (514.6)	19.0	8.6	19.2 (1704.5)	10.1	10.1
Q5 ^f	0.075/0.40/0.20	3.1	28.0	16.8	39627.3 (429.0)	28.7	15.1	28.9 (2805.2)	17.4	13.1
Q6 ^f	0.075/0.45/0.20	3.1	24.5	14.7	34645.7 (392.7)	24.9	12.9	25.1 (2537.1)	17.8	12.0
Q7 ^f	0.075/0.50/0.20	3.2	23.1	13.5	34010.9 (393.4)	23.8	12.5	23.9 (2281.8)	13.8	11.4
Q8 ^f	0.075/0.40/0.25	3.1	23.5	13.7	37752.6 (429.6)	23.9	12.5	24.0 (2333.3)	16.3	10.8

^a At 1000 cd m⁻².

^b The data in the bracket are the corresponding current density.

^c At 3000 cd m⁻².

^d The corresponding luminance.

^e Ir(ppy)₂(acac) red phosphor.

^f Ir(MCPPZ)₃ red phosphor.

smooth, even at 1000 cd m⁻² it still remains 28.0 cd A⁻¹ and 16.8 lm W⁻¹; at 3000 cd m⁻² it remains 28.7 cd A⁻¹ and 15.1 lm W⁻¹, higher than the TCTA or ^tBu-OXDTEFA WOLEDs [50,51]. Moreover, the brightness of our RGBO WOLEDs has obtained general enhancement compared with the RGB series, whose maximum brightness reached around 34010.9–39627.3 cd m⁻². Based on our experimental results, this RGBO white system, with doping ratio of around (10:0.075:0.40:0.20)–(10:0.075:0.50:0.20) for the BGRO components, reaches the highest performance, since the color-quality and EL performance have reached the optimal. For solid-state lighting source, all the photons can be used by reflecting the light to the forward direction through a special lamp fixture, and thus a factor of 1.7–2.3 can be applied to count the total efficiency [30,52,53]. Under this condition, our WOLEDs possess a total power efficiency of 33.6 lm W⁻¹ at 1000 cd m⁻², and 30.2 lm W⁻¹ at 3000 cd m⁻², approaching the state-of-the-art efficiency of fluorescent-tube (40–70 lm W⁻¹) [54].

3.7. Electroluminescent mechanism

In general, two mechanisms regarding single layer WOLEDs are the energy transfer mechanism and the charge carrier trapping mechanism. From the energy level alignment shown in Fig. 1, it can be inferred that carrier trapping mechanism is possible for the energy level difference between HOMO and LUMO of the dopant and host, especially for the long-wave emitting red phosphor. With a 0.4 eV energy difference, holes can be easily trapped on the red dopant molecule, while electrons are resonantly injected in the LUMO orbit from the adjacent TPBI electron transporting layer, followed by direct hole–electron recombination in the red dopant molecule site. This work mechanism is denoted as route 2. This

mechanism is also involved in the blue, green, and orange phosphors, on which electron is trapped and recombined with the hole on the host as denoted as the black arrow in Fig. 1.

The trapping mechanism is further supported by singlet carrier devices. The current density–voltage plots are shown in Fig. 10 of the hole-only and electron-only devices. For the hole-only device doped with the red dopant, the current density is a little lower, indicating the hole-trapping effect. The trapped hole hinders hole transporting, but accesses electron flux due to electrical field-induced effect, which is revealed from the current density–voltage curve where a slightly improved current density is witnessed for the electron-only device upon the introduction of the red dopant, as shown in Fig. 10b.

What's more, energy transfer mechanism also exists, owing to the good overlap between the PL and UV–vis spectrum of the DTPAFB host and the dopants. In addition to singlet exciton energy transfer (Förster type, shown in Fig. 2a), triplet–triplet exciton energy transfer through electron–exchange interaction (Dexter type) from the blue phosphor to the red phosphor molecule is also recorded as shown in Fig. 10c and Fig. S3. An enhanced emission from the dopant under electrical excitation occurred as compared with the photoexcitation because of the big triplet energy difference between them, as shown in Fig. 1 marked as route 1. This result is also coincident with transient decay results as shown in Fig. 3.

As a result, both the energy transfer mechanism and trapping mechanism exists in our white OLEDs. Considering the low doping level, the former mechanism is believed to be dominant. Since charge carrier trapping process is detrimental to the EL spectral stability, the doping concentration should be limited to a very low level. Also, Chen and his coworkers well-demonstrated such a

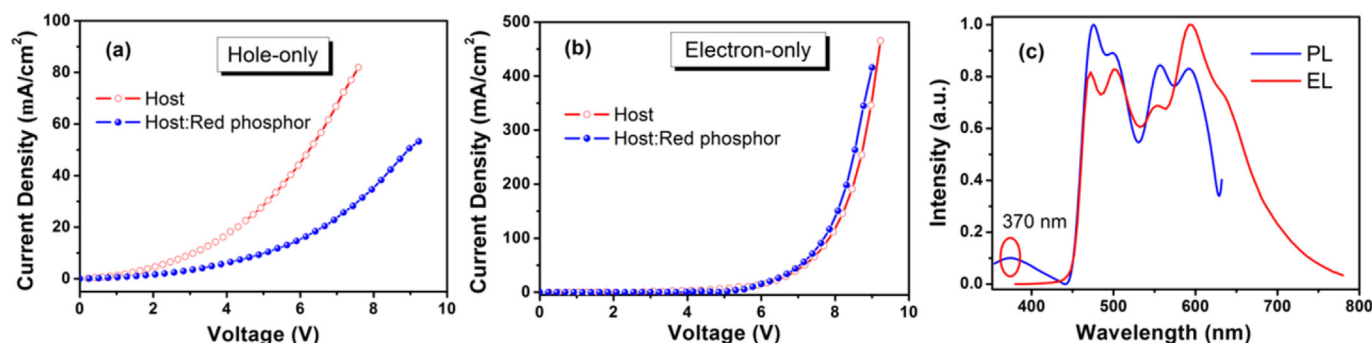


Fig. 10. (a) Current density–voltage characteristic of (a) hole-only and (b) electron-only devices; (c) PL and EL spectrum of the RGBO white OLEDs Q7.

strategy in the recent published review [55]. For all our white OLEDs, the doping content is controlled under 0.50%. For such a low doping level, the trapping effect is confined, as witnessed by the relatively stable EL spectra shown in Fig. 8c, d. So the dominant work mechanism is energy transfer, resulting in relatively stable EL emission. Moreover, the bipolar transportation of the mixed host, the balanced charge injection and transport, and the broad exciton recombination zone in our single emissive layer devices free from interfacial energy barrier, also contribute to this result [56,57].

However, the lifetime of this series white OLED is very short, with only several hours recorded. This is especially serious for the blue phosphorescent device, which is the common problem for solution processed OLEDs, and will be addressed in future studies.

4. Conclusions

We have demonstrated high performance WOLEDs by solution processing method, addressing both aspects of the emission color quality and the EL efficiency. The photophysical properties, energy transfer mechanism between host and guest, surface morphology, and device work mechanism have also been studied. DTPAFB is a sound host material, possessing high triplet energy, suitable HOMO/LUMO energy levels, and excellent film-forming and morphological stability. By carefully combining the commercially available phosphors with the home-made host material, spectrally stable WOLEDs with good color quality have been achieved. The binary BO WOLEDs show stable EL emission with a CRI over 70 and the relatively high EL efficiency of 26.3 cd A^{-1} and power efficiency of 19.6 lm W^{-1} . The optimized RGB WOLEDs show improved CRI up to 81, with maximum luminous efficiency reaching 25.8 cd A^{-1} , 14.4 lm W^{-1} , and EQE of 13.9%. Furthermore, we have achieved high quality white EL emission from RGBO four primary components with a high CRI of 82, and a medium CCT of 3755–3929 K, warm and soft to human eye. The total power efficiency reaches 33.6 lm W^{-1} at 1000 cd m^{-2} , and 30.2 lm W^{-1} at 3000 cd m^{-2} , approaching the state-of-the-art efficiency of fluorescent-tube, potentially suitable for an environment-friendly solid-state lighting source. This kind of work will provide a good guide for further material-choosing and WOLED fabrication.

Acknowledgements

We acknowledge financial support from the National Key Basic Research Program of China (973 Program, 2014CB648300), the National Basic Research Program of China (2012CB933301), the National Nature Science Foundation of China (61106017), the Ministry of Education of China (IRT1148), a Project Funded by the Priority Academic Program Development of Jiangsu Higher Education Institutions (PAPD YX03001), the Jiangsu Government Scholarship for Overseas Studies (JS-2013-221), and the Nature Science Foundation of Jiangsu Province (11KJB430010, BK20131375).

Appendix A. Supplementary data

Supplementary data related to this article can be found at <http://dx.doi.org/10.1016/j.orgel.2016.03.025>.

References

- [1] S. Reineke, F. Lindner, G. Schwartz, N. Seidler, K. Walzer, B. Lussem, K. Leo, *Nature* 459 (2009) 234.
- [2] J.H. Seo, S.J. Lee, B.M. Seo, S.J. Moon, K.H. Lee, J.K. Park, S.S. Yoon, Y.K. Kim, *Org. Electron.* 11 (2010) 1759.
- [3] C. Adachi, M.A. Baldo, M.E. Thompson, S.R. Forrest, *J. Appl. Phys.* 90 (2001) 5048.
- [4] Q. Wang, J.Q. Ding, D.G. Ma, Y.X. Cheng, L.X. Wang, X.B. Jing, F.S. Wang, *Adv. Funct. Mater.* 19 (2009) 84.
- [5] M.C. Gather, A. Koehnen, K. Meerholz, *Adv. Mater.* 23 (2011) 233.
- [6] Q. Wang, Y.H. Chen, J.S. Chen, D.G. Ma, *Appl. Phys. Lett.* 101 (2012) 133302.
- [7] S. Hoffe, A. Schienle, C. Bernhard, M. Bruns, U. Lemmer, A. Colmann, *Adv. Mater.* 26 (2014) 5155.
- [8] F.W. Guo, D.G. Ma, *Appl. Phys. Lett.* 87 (2005) 173510.
- [9] G.Y. Zhong, Y.Q. Zhang, X.A. Cao, *Org. Electron.* 11 (2010) 1338.
- [10] M.C. Gather, A. Koehnen, K. Meerholz, *Adv. Mater.* 23 (2011) 233.
- [11] F.C. Chen, Y. Yang, M.E. Thompson, J. Kido, *Appl. Phys. Lett.* 80 (2002) 2308.
- [12] L. Ying, C.L. Ho, H.B. Wu, Y. Cao, W.Y. Wong, *Adv. Mater.* 26 (2014) 2459.
- [13] K.S. Yook, J.Y. Lee, *Adv. Mater.* 26 (2014) 4218.
- [14] C.W. Lee, J.Y. Lee, *Adv. Mater.* 25 (2013) 596.
- [15] H.B. Wu, J.H. Zou, F. Liu, L. Wang, A. Mikhailovsky, G.C. Bazan, W. Yang, Y. Cao, *Adv. Mater.* 20 (2008) 696.
- [16] H.B. Wu, G.J. Zhou, J.H. Zou, C.L. Ho, W.Y. Wong, W. Yang, J.B. Peng, Y. Cao, *Adv. Mater.* 21 (2009) 4181.
- [17] B.H. Zhang, G.P. Tan, C.S. Lam, B. Yao, C.L. Ho, L.H. Liu, Z.Y. Xie, W.Y. Wong, J.Q. Ding, L.X. Wang, *Adv. Mater.* 24 (2012) 1873.
- [18] Y. Li, K. Xu, X. Wen, L. Zhang, Y. Yin, S. Liu, X. Piao, W. Xie, *Org. Electron.* 14 (2013) 1946.
- [19] J.S. Wang, X.J. Xu, Y. Tian, C. Yao, L.D. Li, *J. Mater. Chem. C* 2 (2014) 5036.
- [20] Y. Li, W. Zhang, L.T. Zhang, X.M. Wen, Y.M. Yin, S.H. Liu, W.F. Xie, H.Y. Zhao, S.L. Tao, *Org. Electron.* 14 (2013) 3201.
- [21] J. Yu, Y. Yin, W. Liu, W. Zhang, L. Zhang, W. Xie, H. Zhao, *Org. Electron.* 15 (2014) 2817.
- [22] S.L. Gong, N. Sun, J.J. Luo, C. Zhong, D.G. Ma, J.G. Qin, C.L. Yang, *Adv. Funct. Mater.* 24 (2014) 5710.
- [23] S. Hoffe, A. Schienle, C. Bernhard, M. Bruns, U. Lemmer, A. Colmann, *Adv. Mater.* 26 (2014) 5155.
- [24] S.H. Ye, Y.Q. Liu, K. Lu, W.P. Wu, C.Y. Du, Y. Liu, H.T. Liu, T. Wu, G. Yu, *Adv. Funct. Mater.* 20 (2010) 3125.
- [25] X. Gong, H. Benmansour, G.C. Bazan, A.J. Heeger, *J. Phys. Chem. B* 110 (2006) 7344.
- [26] B.H. Tong, Q.B. Mei, S.J. Wang, Y. Fang, Y.Z. Meng, B. Wang, *J. Mater. Chem.* 18 (2008) 1636.
- [27] S.J. Su, Y. Takahashi, T. Chiba, T. Takeda, J. Kido, *Adv. Funct. Mater.* 19 (2009) 1260.
- [28] S.J. Su, C. Cai, J. Kido, *J. Mater. Chem.* 22 (2012) 3447.
- [29] H. Huang, X. Yang, Y. Wang, B. Pan, L. Wang, J. Chen, D. Ma, C. Yang, *Org. Electron.* 14 (2013) 2573.
- [30] Y.R. Sun, N.C. Giebink, H. Kanno, B.W. Ma, M.E. Thompson, S.R. Forrest, *Nature* 440 (2006) 908.
- [31] G. Schwartz, M. Pfeiffer, S. Reineke, K. Walzer, K. Leo, *Adv. Mater.* 19 (2007) 3672.
- [32] C. Weichsel, S. Reineke, M. Furno, B. Lussem, K. Leo, *J. Appl. Phys.* 111 (2012) 033102.
- [33] R.J. Holmes, B.W. D'Andrade, S.R. Forrest, X. Ren, J. Li, M.E. Thompson, *Appl. Phys. Lett.* 83 (2003) 3818.
- [34] X. Gong, W.L. Ma, J.C. Ostrowski, G.C. Bazan, D. Moses, A.J. Heeger, *Adv. Mater.* 16 (2004) 615.
- [35] C.W. Seo, J.Y. Lee, *Org. Electron.* 12 (2011) 1459.
- [36] Y.T. Chang, T.H. Jen, S.A. Chen, *Org. Electron.* 14 (2013) 2948.
- [37] T. Peng, Y. Yang, H. Bi, Y. Liu, Z. Hou, Y. Wang, *J. Mater. Chem.* 21 (2011) 3551.
- [38] P.I. Shih, C.Y. Chuang, C.H. Chien, E.W.G. Diau, C.F. Shu, *Adv. Funct. Mater.* 17 (2007) 3141.
- [39] K.S. Yook, J.Y. Lee, *Org. Electron.* 12 (2011) 1293.
- [40] C.-H. Chang, C.-C. Chen, C.-C. Wu, S.-Y. Chang, J.-Y. Hung, Y. Chi, *Org. Electron.* 11 (2010) 266.
- [41] M.H. Ho, S.F. Hsu, J.W. Ma, S.W. Hwang, P.C. Yeh, C.H. Chen, *Appl. Phys. Lett.* 91 (2007) 113518.
- [42] Y. Yang, T. Peng, K. Ye, Y. Wu, Y. Liu, Y. Wang, *Org. Electron.* 12 (2011) 29.
- [43] K.S. Yook, S.O. Jeon, C.W. Joo, J.Y. Lee, M.S. Kim, H.S. Choi, S.J. Lee, C.W. Han, Y.H. Tak, *Org. Electron.* 10 (2009) 681.
- [44] X.F. Ren, J. Li, R.J. Holmes, P.I. Djurovich, S.R. Forrest, M.E. Thompson, *Chem. Mater.* 16 (2004) 4743.
- [45] M.S. Park, H.J. Park, O.Y. Kim, J.Y. Lee, *Org. Electron.* 14 (2013) 1504.
- [46] Z.R. Hong, C.J. Liang, R.G. Li, W.L. Li, D. Zhao, D. Fan, D.Y. Wang, B. Chu, F.X. Zang, L.S. Hong, S.T. Lee, *Adv. Mater.* 13 (2001) 1241.
- [47] K. Xue, B. Chen, G. Han, Y. Duan, P. Chen, Y. Yang, Y. Duan, X. Wang, Y. Zhao, *Org. Electron.* 22 (2015) 122.
- [48] S. Chen, G. Tan, W.-Y. Wong, H.-S. Kwok, *Adv. Funct. Mater.* 21 (2011) 3785.
- [49] Y. Yin, X. Piao, Y. Li, Y. Wang, J. Liu, K. Xu, W. Xie, *Appl. Phys. Lett.* 101 (2012) 063306.
- [50] C.C. Fan, M.H. Huang, W.C. Lin, H.W. Lin, Y. Chi, H.F. Meng, T.C. Chao, M.R. Tseng, *Org. Electron.* 15 (2014) 517.
- [51] C.H. Chien, L.R. Kung, C.H. Wu, C.F. Shu, S.Y. Chang, Y. Chi, *J. Mater. Chem.* 18 (2008) 3461.
- [52] B.W. D'Andrade, R.J. Holmes, S.R. Forrest, *Adv. Mater.* 16 (2004) 624.
- [53] X. Gong, S. Wang, D. Moses, G.C. Bazan, A.J. Heeger, *Adv. Mater.* 17 (2005) 2053.
- [54] H.B. Wu, L. Ying, W. Yang, Y. Cao, *Chem. Soc. Rev.* 38 (2009) 3391.
- [55] S. Chen, Q. Wu, M. Kong, X. Zhao, Z. Yu, P. Jia, W. Huang, *J. Mater. Chem. C* 1 (2013) 3508.
- [56] M.C. Gather, R. Alle, H. Becker, K. Meerholz, *Adv. Mater.* 19 (2007) 4460.
- [57] C.-H. Hsiao, S.-W. Liu, C.-T. Chen, J.-H. Lee, *Org. Electron.* 11 (2010) 1500.